Monthly Notices
of the
ROYAL ASTRONOMICAL SOCIETY

MNRAS **467,** 971–984 (2017)
Advance Access publication 2017 January 19

doi:10.1093/mnras/stx144

ZASPE: a code to measure stellar atmospheric parameters and their covariance from spectra

Rafael Brahm,[1,2]★ Andrés Jordán,[1,2] Joel Hartman[3] and Gáspár Bakos[3]†‡

[1]*Instituto de Astrofísica, Facultad de Física, Pontificia Universidad Católica de Chile, Av. Vicuña Mackenna 4860, 7820436 Macul, Santiago, Chile*
[2]*Millennium Institute of Astrophysics, Santiago, Chile*
[3]*Department of Astrophysical Sciences, Princeton University, Princeton, NJ 08544, USA*

Accepted 2017 January 17. Received 2017 January 13; in original form 2015 December 7

ABSTRACT

We describe the Zonal Atmospheric Stellar Parameters Estimator (ZASPE), a new algorithm, and its associated code, for determining precise stellar atmospheric parameters and their uncertainties from high-resolution echelle spectra of FGK-type stars. ZASPE estimates stellar atmospheric parameters by comparing the observed spectrum against a grid of synthetic spectra only in the most sensitive spectral zones to changes in the atmospheric parameters. Realistic uncertainties in the parameters are computed from the data itself, by taking into account the systematic mismatches between the observed spectrum and the best-fitting synthetic one. The covariances between the parameters are also estimated in the process. ZASPE can in principle use any pre-calculated grid of synthetic spectra, but unbiased grids are required to obtain accurate parameters. We tested the performance of two existing libraries, and we concluded that neither is suitable for computing precise atmospheric parameters. We describe a process to synthesize a new library of synthetic spectra that was found to generate consistent results when compared with parameters obtained with different methods (interferometry, asteroseismology, equivalent widths).

Key words: methods: data analysis – techniques: spectroscopic – stars: fundamental parameters – planetary systems.

1 INTRODUCTION

The determination of the physical parameters of stars is a fundamental requirement for studying their formation, structure and evolution. Additionally, the physical properties of extrasolar planets depend strongly on how well we have characterized their host stars. In the case of transiting planets, the measured transit depth is related to the ratio of the planet to stellar radii. Similarly, for radial velocity planets, the semi-amplitude of the orbit is a function of both the mass of the star and the mass of the planet. In the case of directly imaged exoplanets, their estimated masses depend on the age of the systems. With more than 3000 planets and planetary candidates discovered, mostly by the *Kepler* mission (e.g. Howard et al. 2012; Burke et al. 2014), homogeneous and accurate determination of the physical parameters of the host stars are required for linking their occurrence rates and properties with different theoretical predictions (e.g. Howard et al. 2010; Buchhave et al. 2014).

Direct determinations of the physical properties of single stars (mass, radius and age) are limited to a couple dozens of systems. Long baseline optical interferometry has been used on bright sources with known distances to measure their physical radii (Boyajian et al. 2012, 2013) and precise stellar densities have been obtained using asteroseismology on stars observed by *Kepler* and *CoRoT* (e.g. Silva Aguirre et al. 2015). Unfortunately, for the rest of the stars, including the vast majority of planetary hosts, physical parameters cannot be measured and indirect procedures have to be adopted in which the atmospheric parameters, such as the effective temperature ($T_{\rm eff}$), surface gravity ($\log g$) and metallicity ([Fe/H]), are derived from stellar spectra by using theoretical model atmospheres. Stellar evolutionary models are then compared with the estimated atmospheric parameters in order to determine the physical parameters of the star.

The amount of information about the properties of the stellar atmosphere contained in its spectrum is enormous. Current state-of-the-art high-resolution echelle spectrographs are capable of detecting subtle variations of spectral lines that, in principle, can be translated into the determination of the physical atmospheric conditions of a star with exquisite precision. However, there are several factors that reduce the precision that can be achieved. On one side, there are many other properties of a star that can produce changes on the absorption lines. For example, velocity fields on the surface of the star, which include the stellar rotation (which may be differential) and the micro- and macroturbulence, modify the shape

★ E-mail: rbrahm@gmail.com
† Alfred P. Sloan Research Fellow.
‡ Packard Fellow.

of the absorption lines. Non-solar abundances change the particular strength of the lines of each element. Therefore, in order to obtain precise atmospheric parameters, all of these variables have to be considered. However, even when all the significant variables of the problem are taken into account, the precision in the parameters becomes limited by modelling uncertainties, e.g. imperfect modelling of the stellar atmospheres and spectral features due to unknown opacity distribution functions, uncertainties in the properties of particular atomic and molecular transitions, effects arising from the assumed geometry of the modelled atmosphere and non-local thermodynamic equilibrium (LTE) effects. These sources of error are unavoidable and are currently the main problem for obtaining reliable uncertainties in the estimated stellar parameters. Most of the actual algorithms that compute atmospheric parameters from high-resolution stellar spectra do not consider in detail this factor for obtaining the uncertainties. The problem is that if the reported uncertainties are unreliable, then they propagate to the planetary parameters and can bias the results or hide potential trends in the properties of the system under study that, if detectable, could lead to deeper insights into their formation and evolution.

A widely used procedure for obtaining the atmospheric parameters of a star consists in comparing the observed spectra against synthetic models and adopts the parameters of the model that produces the best match as the estimated atmospheric parameters of the observed star. This technique has been implemented in algorithms such as SME (Valenti & Piskunov 1996), SPC (Buchhave et al. 2012) and ISPEC (Blanco-Cuaresma et al. 2014) to derive parameters of planetary host stars. Thanks to the large number of spectral features used, this method has been shown to be capable of dealing with spectra having low signal-to-noise ratio (SNR), moderate resolution and a wide range of stellar atmospheric properties. However, one of the major drawbacks of spectral synthesis methods for the estimation of the atmospheric parameters is the determination of their uncertainties. This problem arises because the source of error is not the Poisson noise of the observed spectrum, but instead is usually dominated by imperfections in the synthesized model spectra, which produce highly correlated residuals. In such cases, standard procedures for computing uncertainties for the parameters are not reliable. For example, SPC computes the internal uncertainties using the dispersion from different measurements in the low SNR regime, but an arbitrary floor is applied when the uncertainties are expected to be dominated by the systematic missmatches between models and data. Additionally, Torres et al. (2012) showed that there are strong correlations between the atmospheric parameters obtained using spectral synthesis techniques, and therefore, the covariance matrix of the parameters should be a required output of any stellar parameter classification tool so that the uncertainty of its results is properly propagated to the posterior inferences that are made using them. Recently, Czekala et al. (2015) introduced STARFISH, a code that allows robust estimation of stellar parameters using synthetic models by using a likelihood function with a covariance structure described by Gaussian processes. STARFISH allows robustness to synthetic model imperfections through a principled approach using a sophisticated likelihood function and provides full posterior distributions for the parameters, but as we will argue later its uncertainties are significantly underestimated.

In this paper, we present a new algorithm, dubbed Zonal Atmospheric Stellar Parameters Estimator (ZASPE)[1] for estimating stellar atmospheric parameters using the spectral synthesis technique. The uncertainties and correlations in the parameters are computed from the data itself and include the systematic mismatches due to the imperfect nature of the theoretical spectra. The structure of the paper is as follows. In Section 2, we describe the method that ZASPE uses for determining the stellar parameters and their covariance matrix, including details on the synthesis of a new synthetic library to overcome limitations of the existing libraries for stellar parameter estimation. In Section 3, we summarize the performance of ZASPE on a sample of stars with measured stellar parameters, and we compare our uncertainties with those produced by STARFISH. Finally, in Section 4, we summarize and conclude.

2 THE METHOD

In order to determine the atmospheric stellar parameters of a star, ZASPE compares an observed continuum normalized spectrum against synthetic spectra using least-squares minimization by performing an iterative algorithm that explores the complete parameter space of FGK-type stars. For simplicity, we assume first that we are able to generate an unbiased synthetic spectrum with any set of stellar atmospheric parameters ($T_{\rm eff}$, $\log g$ and [Fe/H]). By unbiased, we mean that there are no systematic trends in the level of mismatch of the synthesized and real spectra as a function of the stellar parameters, but there can be systematic mismatches that are not a function of stellar parameters. If F_λ is the observed spectrum and $S_\lambda(\boldsymbol{\theta})$ is the synthesized spectrum with parameters $\boldsymbol{\theta} = \{T_{\rm eff}, \log g, [{\rm Fe/H}]\}$, the quantity that we minimize is

$$X^2(\boldsymbol{\theta}) = \sum_\lambda (F_\lambda - S_\lambda(\boldsymbol{\theta}))^2. \quad (1)$$

In equation (1), we have not included the weights coming from the uncertainties in the observed flux because we are assuming that the SNR of the data is high enough for the uncertainties in the parameters to be governed by the systematic mismatches between the data and the models.

The synthesized spectrum needs to have some processing done in order to compare it against the observed one. We do not treat microturbulence and macroturbulence as free parameters, but instead we assume that these values are functions of the atmospheric parameters. The microturbulence value is required during the process of synthesizing the spectra and it depends on the particular spectral library selected to do the comparison (see Section 2.6). On the other hand, the macroturbulence degradation is applied after the synthetic spectra have been generated. We compute the macroturbulence value for each synthetic spectrum from its $T_{\rm eff}$ using the empirical relation given in Valenti & Fischer (2005),[2] namely,

$$v_{\rm mac} = \left(3.98 + \frac{T_{\rm eff} - 5770\,{\rm K}}{650\,{\rm K}}\right)\ {\rm km\,s^{-1}}. \quad (2)$$

The effect of macroturbulence on the spectrum is given by a convolution with a Gaussian kernel whose standard deviation is given by $\sigma_{\rm mac} = 0.297 v_{\rm mac}$, as was approximated in Takeda, Sato & Murata (2008). The degradation to the particular instrumental resolution, $R = \Delta\lambda/\lambda$, is performed by convolving the synthetic spectrum with another Gaussian kernel whose standard deviations is $\sigma_{\rm res} = \lambda/(2.3R)$. The model spectrum is then split according to the echelle orders of the observed spectrum and the pixelization effect is taken into account by integrating the synthetic flux over each wavelength element of the observed spectrum.

[1] The code can be found on http://github.com/rabrahm/zaspe.

[2] As was pointed out by Torres et al. (2012), the formula in Valenti & Fischer (2005) has a wrong sign.

2.1 The sensitive zones

One of the novel features of ZASPE in contrast to other similar codes is that the comparison between the observed and synthetic spectra is performed in particular optimized wavelength zones, rather than using the full spectrum. These zones correspond to the most sensitive regions of the spectra to changes in the stellar parameters and are redefined in each iteration of ZASPE.

These sensitive regions are determined from the approximate gradient of the modelled spectra with respect to the stellar parameters at $\boldsymbol{\theta}^{\rm c}$, where $\boldsymbol{\theta}^{\rm c} = \{T_{\rm eff}^{\rm c}, \log g^{\rm c}, [{\rm Fe/H}]^{\rm c}\}$ is the set of parameters that produced the minimum X^2 in the previous iteration. In practice, once $\boldsymbol{\theta}^{\rm c}$ is determined, ZASPE computes the following finite differences:

$$\Delta S^1_{T_{\rm eff}} = \|S_\lambda(T_{\rm eff}^{\rm c} + 200, \log g^{\rm c}, [{\rm Fe/H}]^{\rm c}) - S_\lambda(\boldsymbol{\theta}^{\rm c})\|, \quad (3)$$

$$\Delta S^2_{T_{\rm eff}} = \|S_\lambda(T_{\rm eff}^{\rm c} - 200, \log g^{\rm c}, [{\rm Fe/H}]^{\rm c}) - S_\lambda(\boldsymbol{\theta}^{\rm c})\|, \quad (4)$$

$$\Delta S^1_{\log g} = \|S_\lambda(T_{\rm eff}^{\rm c}, \log g^{\rm c} + 0.3, [{\rm Fe/H}]^{\rm c}) - S_\lambda(\boldsymbol{\theta}^{\rm c})\|, \quad (5)$$

$$\Delta S^2_{\log g} = \|S_\lambda(T_{\rm eff}^{\rm c}, \log g^{\rm c} - 0.3, [{\rm Fe/H}]^{\rm c}) - S_\lambda(\boldsymbol{\theta}^{\rm c})\|, \quad (6)$$

$$\Delta S^1_{[{\rm Fe/H}]} = \|S_\lambda(T_{\rm eff}^{\rm c}, \log g^{\rm c}, [{\rm Fe/H}]^{\rm c} + 0.2) - S_\lambda(\boldsymbol{\theta}^{\rm c})\|, \quad (7)$$

$$\Delta S^2_{[{\rm Fe/H}]} = \|S_\lambda(T_{\rm eff}^{\rm c}, \log g^{\rm c}, [{\rm Fe/H}]^{\rm c} - 0.2) - S_\lambda(\boldsymbol{\theta}^{\rm c})\| \quad (8)$$

from which the approximate gradient of the synthesized spectra with respect to the atmospheric parameters, averaged on the three parameters, is estimated as

$$\Delta S_\lambda(\boldsymbol{\theta}^{\rm c}) = \frac{1}{6}(\Delta S^1_{T_{\rm eff}} + \Delta S^2_{T_{\rm eff}} + \Delta S^1_{\log g} + \Delta S^2_{\log g} + \Delta S^1_{[{\rm Fe/H}]} + \Delta S^2_{[{\rm Fe/H}]}). \quad (9)$$

Spectral regions where $\Delta S_\lambda(\boldsymbol{\theta}^{\rm c})$ is greater than a predefined threshold are identified as the sensitive zones, which we denote as $\{z_i\}$. Fig. 1 shows a portion of the spectrum for three different stars and the sensitive zones selected in the final ZASPE iteration in each case. It can be seen that the selected sensitive zones correspond to the spectral regions where absorption lines are present, but that not all the absorption lines are identified as sensitive zones at a given threshold. In addition, the regions that are selected as sensitive zones vary according to the properties of the observed star. For identifying the sensitive zones, we have introduced four quantities that take arbitrary values. These correspond to the distance in step sizes for the three atmospherical parameters (200 K, 0.3 dex and 0.2 dex for $T_{\rm eff}$, $\log g$ and [Fe/H], respectively) that are used to compute the gradient of the grid, and the threshold value (0.09 as default) that defines as sensitive zones the spectral regions where the gradient is greater than this value. The particular values that we selected as default allow ZASPE to identify a great number of sensitive zones even for F-type stars, but at the same time, each of these zones contains just one or two significant absorption lines even in the case of the crowded K-type stars. This last requirement is mandatory for the procedure that ZASPE uses to compute the errors in the parameters (see Section 2.5).

The introduction of the zones into the problem also allows the rejection of portions of the spectra that strongly deviate from $S_\lambda(\boldsymbol{\theta}^{\rm c})$, due to modelling problems or by the presence of artefacts in the data that remain in the spectrum (e.g. cosmic rays and bad columns). In practise, outliers are identified by computing the root mean square (rms) of the residuals between the observed spectra and the optimal synthetic one in each sensitive zone and zones with rms values

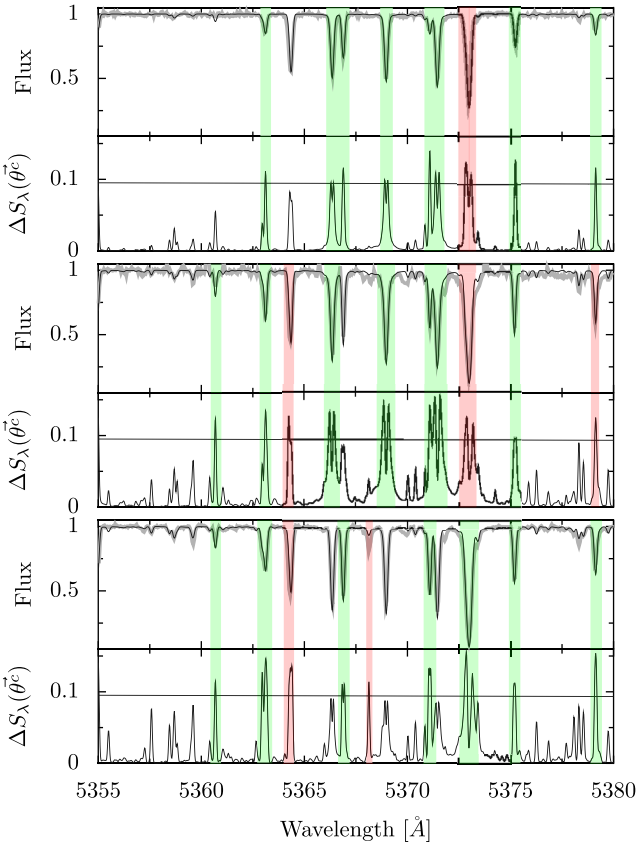

Figure 1. Sensitive zones determined by ZASPE in a portion of the wavelength coverage for three different stars (top panel: late F-dwarf; central panel: solar-type star; bottom panel: K-giant). In each panel, the superior plot corresponds to the observed spectrum (thick line) and the optimal synthetic one determined by ZASPE (thin line), while the inferior plot shows the gradient $\Delta S_\lambda(\boldsymbol{\theta}^{\rm c})$ of the synthetic grid evaluated at the parameters of the optimal synthetic spectrum, and the threshold (horizontal line) that determines which regions of the spectrum are defined as sensitive zones. The green coloured regions correspond to the sensitive zones determined by ZASPE where the comparison between data and models is performed. The red coloured regions are regions of the spectrum that are initially identified as sensitive zones by ZASPE but then rejected because the average residual between the optimal model and the data in these particular regions is significantly higher (greater than 3σ) than in the rest of the sensitive zones.

greater than three times the average rms value are rejected. Once the sensitive zones are known, ZASPE builds a binary mask, M_λ, filled with ones in the spectral range of the sensitive zones and zeros elsewhere, i.e.

$$M_\lambda = \begin{cases} 1 : \lambda \in \{z_n\}, \\ 0 : \lambda \notin \{z_n\}. \end{cases} \quad (10)$$

For the next iteration, the function to be minimized will be

$$X^2(\boldsymbol{\theta}) = \sum_\lambda M_\lambda (F_\lambda - S_\lambda(\boldsymbol{\theta}))^2. \quad (11)$$

In the first iteration of ZASPE the complete spectral range is utilized and $M_\lambda \equiv 1 \, \forall \, \lambda$.

2.2 Continuum normalization

ZASPE contains an algorithm that performs the continuum normalization of the observed spectra, which is required for a proper comparison with the synthetic spectral library. One important assumption

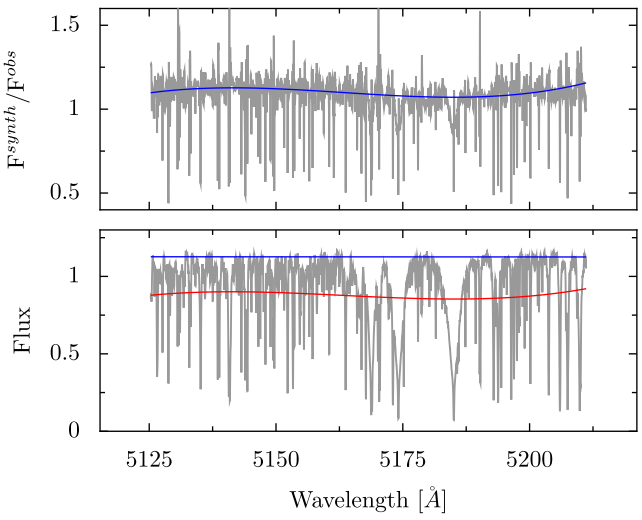

Figure 2. Top: the blue line corresponds to the polynomial fitted to the ratio between the optimal synthetic spectrum find in the previous ZASPE iteration and the observed spectrum. This procedure allows us to determine the continuum normalization without overfitting wide spectral features. Bottom: comparison between the continuum determined by the algorithm that ZASPE uses (blue line) and the one determined by fitting a simple polynomial (red line), which clearly is heavily affected by the presence of strong absorption features.

that we make at this step is that the large-scale variations of the observed flux as function of wavelength must be smooth and it must be possible to accurately trace them with a simple low-degree polynomial. This means that the observed spectrum should be at least corrected by the blaze function, and it should not contain systematics in order to define a proper continuum or pseudocontinuum. If the input observed spectrum satisfies this constrain, then our continuum normalization algorithm deals with the presence of both, shallow and strong spectral features. The continuum is updated after each ZASPE iteration, because the optimal model is used by the algorithm to avoid an overfitting of the wide spectral features, like the zone of the Mg Ib triplet for example. The idea is to bring the continuum of the observed spectrum to match the continuum of the optimal synthetic one. Therefore, for every echelle order, the optimal synthetic spectrum found after each ZASPE iteration is divided by the observed spectrum, and polynomials are fitted to these ratios using an iterative procedure that rejects regions where the model and data significantly differ. Given that both model and data should contain the wide spectral features, these disappear when the division is performed, and the only significant features that remain are the instrumental response and the blackbody wavelength dependence of the observed spectrum. The polynomials obtained for each echelle order are then multiplied by the observed spectrum, which corrects for the large-scale smooth variations. Finally, a straight line is fitted to this corrected spectrum using an iterative process that excludes the absorption lines from the fit. This last normalization is applied to ensure that the continuum or pseudo-continuum takes values equal to 1, which is particularly important when determining and applying the mismatch factors of Section 2.5. Additionally, the synthetic spectra are also normalized by a straight line. Fig. 2 shows that the normalization algorithm used by ZASPE performs better in zones with wide spectral features than a simple polynomial fit. The observed spectrum in the lower panel of Fig. 2 has already been corrected for the large-scale variations using the information provided by the best-fitting synthetic model shown in the upper panel. The red line in the lower panel shows that a simple polynomial fit is heavily affected by the strong absorption features even after removing large-scale variations.

2.3 Radial velocity and $v \sin i$

In each ZASPE iteration, the search of the X^2 minimum is performed simultaneously over the three atmospheric parameters. However, the velocity of the observed spectrum with respect to the synthesized spectra (radial velocity) and the $v \sin i$ value are updated in each ZASPE iteration after $\boldsymbol{\theta}^{\rm c}$ is determined, because of the slight dependence of these quantities to the atmospheric parameters. In practise, the radial velocity and $v \sin i$ of the observed spectrum are obtained from the cross-correlation function computed between the observed spectrum and the synthesized one with parameters $\boldsymbol{\theta}^{\rm c}$ and $v \sin i = 0$ km s^{-1}. This cross-correlation function is given by

$$\mathrm{CCF}(v, 0) = \int M_\lambda F_\lambda S_{\lambda'}(\boldsymbol{\theta}^{\rm c}, 0)\, \mathrm{d}\lambda, \tag{12}$$

where λ' is the Doppler shifted wavelength by a velocity v, given in the non-relativistic regime by $\lambda' = \lambda + \lambda v/c$, where c is the speed of light. A Gaussian function is fitted to the CCF and the mean of the Gaussian is assumed as the radial velocity of the observed spectrum, while the $v \sin i$ is determined from the full width at half-maximum (FWHM) of the CCF peak as follows. New CCFs are computed between the synthetic spectrum without rotation and the same synthetic spectrum degraded by different amounts of $v \sin i$:

$$\mathrm{CCF}(v, v \sin i) = \int M_\lambda S_\lambda(\boldsymbol{\theta}^{\rm c}, v \sin i) S_{\lambda'}(\boldsymbol{\theta}^{\rm c}, 0)\, \mathrm{d}\lambda. \tag{13}$$

The FWHM is computed for each CCF peak and a cubic spline is fitted to the relation between the FWHM and $v \sin i$ values. This cubic spline is then used to find the $v \sin i$ of the observed spectra from the FWHM of the CCF computed in equation (12).

In the next ZASPE iteration, all the synthesized spectra are degraded to the $v \sin i$ obtained in the previous iteration, and the observed spectrum is corrected in radial velocity by the amount found from the cross-correlation function. The degradation of the spectrum by rotation is performed with a rotational kernel computed following equation (18.11) of Gray (2008). The convolution of the synthetic spectra with a rotational kernel corresponds to an integration of the stellar intensity over the stellar disc. The stellar disc has different velocity components at different points of the disc, and thus the effects of limb darkening have to be considered when performing the convolution. The limb darkening is modelled by using the quadratic limb-darkening law with coefficients for the appropriate stellar parameters calculated using the code from Espinoza & Jordán (2015). The $v \sin i$ value for the first ZASPE iteration is obtained by cross-correlating the observed spectrum against one with stellar parameters similar to those of the Sun.

2.4 Grid exploration

The synthesis of high-resolution spectra is a computationally intensive process. For this reason, ZASPE uses a pre-computed grid of synthetic spectra and, in order to obtain a synthetic spectrum for an arbitrary set of stellar parameters, a cubic multidimensional interpolation is performed.

Given the known correlations between the three atmospheric parameters and the possibility of existence of secondary minima in X^2 space due to the imperfect modelling of the synthetic spectra, the approach of ZASPE for finding the global X^2 minimum is to explore

Table 1. Grid extension and spacing for each ZASPE iteration.

Iteration	$T_{\rm eff}^{\rm i}$ (K)	$T_{\rm eff}^{\rm f}$ (K)	$\Delta T_{\rm eff}$ (K)	$\log g^{\rm i}$	$\log g^{\rm f}$	$\Delta \log g$	$[{\rm Fe/H}]^{\rm i}$	$[{\rm Fe/H}]^{\rm f}$	$\Delta[{\rm Fe/H}]$
1	4000	7000	200	1.0	5.0	0.5	−1.0	0.5	0.5
2	$T_{\rm eff}^{\rm c} - 500$	$T_{\rm eff}^{\rm c} + 500$	100	$\log g^{\rm c} - 0.6$	$\log g^{\rm c} + 0.6$	0.2	$[{\rm Fe/H}]^{\rm c} - 0.4$	$[{\rm Fe/H}]^{\rm c} + 0.4$	0.1
3	$T_{\rm eff}^{\rm c} - 300$	$T_{\rm eff}^{\rm c} + 300$	75	$\log g^{\rm c} - 0.6$	$\log g^{\rm c} + 0.6$	0.2	$[{\rm Fe/H}]^{\rm c} - 0.3$	$[{\rm Fe/H}]^{\rm c} + 0.3$	0.075
4	$T_{\rm eff}^{\rm c} - 200$	$T_{\rm eff}^{\rm c} + 200$	50	$\log g^{\rm c} - 0.4$	$\log g^{\rm c} + 0.4$	0.1	$[{\rm Fe/H}]^{\rm c} - 0.2$	$[{\rm Fe/H}]^{\rm c} + 0.2$	0.05
>4	$T_{\rm eff}^{\rm c} - 50$	$T_{\rm eff}^{\rm c} + 50$	10	$\log g^{\rm c} - 0.2$	$\log g^{\rm c} + 0.2$	0.05	$[{\rm Fe/H}]^{\rm c} - 0.06$	$[{\rm Fe/H}]^{\rm c} + 0.06$	0.02

the complete parameter space covered by the grid and not to rely on slope minimization techniques that require an initial set of guess parameters.

In each ZASPE iteration, the extension and spacing of the parameter grid being explored changes. In the first iteration, ZASPE explores the complete atmospheric parameter grid with coarse spacing, while from the fourth iteration on, ZASPE starts focusing on smaller regions of parameter space around $\boldsymbol{\theta}^{\rm c}$ that are densely explored. Table 1 shows the extension and spacings ($\Delta T_{\rm eff}$, $\Delta \log g$, Δ[Fe/H]) that ZASPE uses for each iteration in its default version, but these values can be easily modified by the user. We note that while the spacing of the grid decreases after each iteration, the gradient intervals used for identifying the sensitive zones are kept constant through the ZASPE iterations.

ZASPE terminates the iterative process when the parameters obtained after each iteration do not change by significant amounts. In detail, convergence is assumed to be reached when the parameters obtained in the ith iteration do not differ by more than 10 K, 0.03 dex and 0.01 dex in $T_{\rm eff}$, $\log g$ and [Fe/H], respectively, from the ones obtained in the $(i-1)$th iteration. This convergence is usually achieved after ∼5–10 iterations.

2.5 Parameter uncertainties and correlations

As we mentioned in Section 1, one major issue of the algorithms that use spectral synthesis methods for estimating the stellar atmospheric parameters is the problem of obtaining reliable estimates of the uncertainties in the parameters and their covariances. ZASPE deals with this problem by assuming that the principal source of errors is the systematic mismatch between the observed spectrum and the synthetic one. The top panel of Fig. 3 shows a portion of a high-resolution spectrum of a star and the synthetic spectrum that produces the best match with the data. Even though each absorption line is present in both spectra, the depth of the lines is frequently different. This systematic mismatch can be further identified in the central panel of Fig. 3, where the residuals in the regions of the absorption lines can be seen to be in several cases significantly greater than those expected just from photon noise. In addition, the residuals are clearly non-Gaussian and highly correlated in wavelength.

In the case of dealing with Gaussian and uncorrelated residuals, a valid approach to estimate the errors in the parameters would be to perform Monte Carlo simulations in which Gaussian errors are uniformly added to the synthetic models at the level present in the observed spectrum, and new sets of optimal parameters are estimated in several realizations. The errors in the parameters could then be estimated from the distribution of output parameters obtained from the different realizations of the simulation. In our case, we cannot follow directly this approach, but we can use a similar procedure if we are able to properly model the source that dominates the error budget. Our procedure builds upon the approach of Grunhut (2009) and consists in performing Monte Carlo simulations in which, instead of adding Gaussian noise, the depths of the

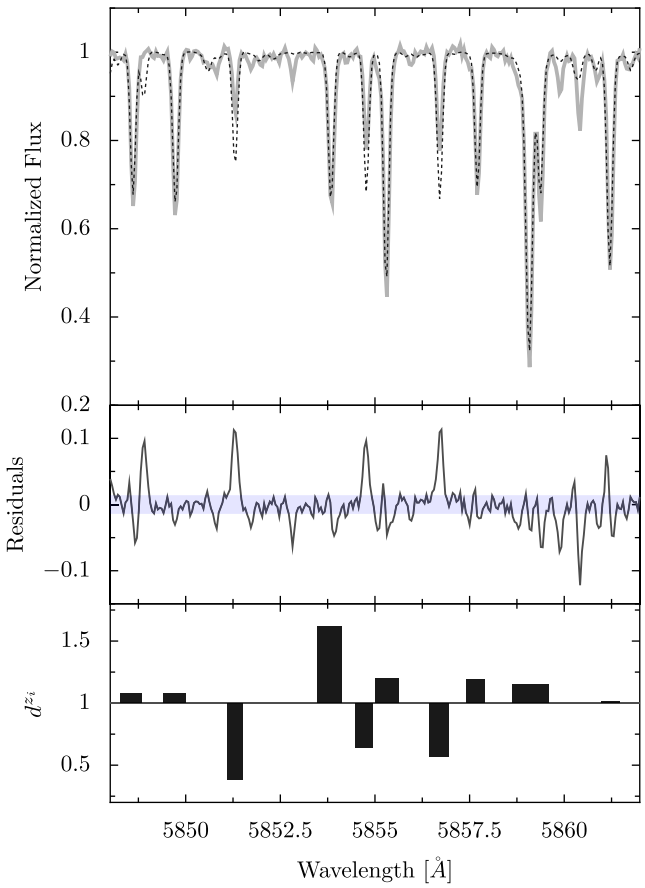

Figure 3. Top: portion of a high-resolution echelle spectrum of a star (continuous line) and the synthetic spectrum that produces the best match with the data (dashed line). Centre: residuals between the two spectra and the expected 3σ errors. Both panels show that the synthetic spectrum that best fits the data produces systematic mismatches in the zones of the absorption lines and that the errors are greater than the ones expected from the received flux. Bottom: mismatch factors d^{z_i} computed in the case of the 10 sensitive zones identified in this portion of the spectrum.

absorption lines of the synthetic spectra are randomly modified at the level of the observed mismatch. In the following paragraphs, we describe in detail how we model the mismatch and how the modification of the spectral lines is performed.

We define a random variable D_i that is responsible for modifying the strength of each absorption feature in a sensitive zone z_i of the synthesized spectrum. If $S_\lambda^{\prime z_i}$ is a perfect synthetic spectrum in the ith sensitive zone z_i, given a probability density $P(D)$ for the random variable D, an imperfect synthetic spectrum $S_\lambda^{z_i}$ (like the ones of the spectral libraries that ZASPE uses) is modelled as

$$S_\lambda^{z_i} = (S_\lambda^{\prime z_i} - 1)D + 1. \quad (14)$$

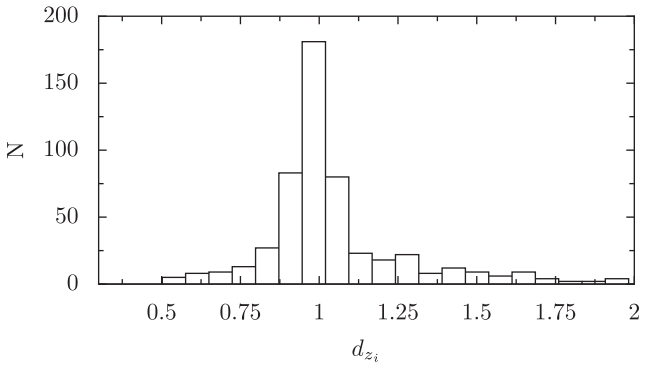

Figure 4. Histogram of the mismatch factors in the sensitive zones. In several regions of the spectrum the absorption lines of the synthetic spectrum can strongly deviate from the ones of the observed one.

An estimate of the probability density function $P(D)$ can be obtained from the data itself by computing the set of mismatch factors, dz_i for all sensitive zones, computed from the difference between the data and the optimal synthetic spectrum found in the final ZASPE iteration. For each sensitive zone, these factors d^{z_i} are obtained from the median value, over all pixels in z_i, of the division between the observed and synthetic spectra:

$$d^{z_i} = \text{median}\left(\frac{F_\lambda^{z_i} - 1}{S_\lambda^{z_i} - 1}\right). \quad (15)$$

The bottom panel of Fig. 3 shows the mismatch factors in the case of the 10 sensitive zones identified in that portion of the spectrum. Fig. 4 shows an histogram of the mismatch factors for the same spectrum of Fig. 3 but for a greater wavelength coverage ($5000 < \lambda < 6000$ Å). The distribution of mismatch factors is pretty symmetric, centred around $d^{z_i} = 1$ and shows a wide spread of values. Most of the absorption lines of the synthetic spectrum that best fits the data have values between 50 per cent and 200 per cent of the strength of the observed ones. Some lines can deviate even more; however, these zones are rejected as strong outliers by ZASPE, as explained in Section 2.1.

ZASPE estimates the probability distribution of the stellar atmospheric parameters by running a random sampling method where a synthetic spectrum that produces the minimum X^2 is searched again a number B of realizations, in the same way as described in the previous sections, but using a modified set of model spectra in each realization. The only difference between the minimization run on each realization and the original search is that the set of sensitive zones $\{z_i\}$ is kept fixed at the set that ZASPE converged to. In each replication, the strength of the lines of the synthetic spectra is modified by randomly selecting mismatch factors from the $\{d^{z_i}\}$ set, with replacement. Each sensitive zone is modified by a different factor that can be repeated, but the same factor is applied in each zone for the whole set of synthesized spectra. In the random sampling method, the quantity that is minimized on each iteration b is

$$X_b^2 = \sum_\lambda M_\lambda (F_\lambda - (S_\lambda(\boldsymbol{\theta}) - 1)D_\lambda + 1)^2, \quad (16)$$

where D_λ is a mask defined for each realization and contains the mismatch factors for each sensitive zone. In order to avoid possible biases in the final distribution of the parameters originating from the asymmetry in the sampling function, when a factor is selected from $\{dz_i\}$ we include a 0.5 probability for this factor to take its reciprocal value, enforcing in practice symmetry in the function from which the factors are sampled. After each realization of the sampling method, a new set of atmospheric parameters is found. From these set of possible outcomes, the complete covariance matrix of the atmospheric parameters can be estimated. After testing the method on spectra with different stellar atmospheric parameters we found that about $B = 100$ realizations are enough to obtain reliable parameter covariance matrices.

The procedure that ZASPE uses to obtain the errors and correlations assumes that the systematic mismatches between the different zones are uncorrelated. This simplification of the problem means that some systematic errors between the data and the models are not accounted for by our method. For example, if the abundance of one particular atomic species strongly deviates from the one assumed in our model, the degree of mismatch of the absorption lines of that element will be correlated. However, in Section 3, we will find that our assumption is able to account for the typical value of systematic errors in atmospheric parameters, as inferred from measuring the parameters with different methods.

2.6 The reference spectral synthetic library

In order to determine the atmospheric stellar parameters of a star, ZASPE compares the observed spectrum against a grid of synthetic models. In principle, after some minor specifications about the particular format of the grid, ZASPE can use any pre-calculated grid. We have tested ZASPE with two publicly available grids of synthetic spectra: the one of Coelho et al. (2005, hereafter C05), which are based in the ATLAS model atmospheres (Kurucz 1993); and the one presented in Husser et al. (2013, hereafter H13), which is based in the PHOENIX model atmospheres. We have found that both grids present important biases when comparing the stellar parameters obtained using them with ZASPE for a set of reference stars. In Fig. 5, we show the comparison of the results obtained by ZASPE against the values presented in SWEET-Cat (Santos et al. 2013) for a set of publicly available spectra in the ESO archive.

SWEET-Cat is a catalogue of atmospheric stellar parameters of planetary host stars. The parameters were computed using the equivalent width method and the ATLAS plane–parallel model atmospheres (Kurucz 1993) on a set of high SNR and high spectral resolution echelle spectra. We decided to use SWEET-Cat for benchmarking our method because (1) it includes stars with a wide range of stellar parameters; (2) the same homogeneous analysis is applied to each spectrum; (3) the equivalent width method has clear physical foundations and does not produce strong correlations between the inferred parameters and (4) the inferred parameters have been shown to be consistent with results obtained with different, less model-dependent methods (infrared flux, interferometry, stellar density computed from transit light-curve modelling) and also with standard spectral synthesis tools like SPC and SME (Torres et al. 2012).

The top panels of Fig. 5 show the comparison of the results obtained by ZASPE using the H13 library. These results deviate strongly from the reference values for the three atmospheric parameters. The parameters are systematically underestimated by 300 K, 0.6 dex and 0.3 dex on average in $T_{\rm eff}$, $\log g$ and [Fe/H], respectively. There also appear to be quadratic trends in $T_{\rm eff}$ and $\log g$ that produce greater deviations for hot and/or giant stars. These systematic trends can be expected from this kind of grid of synthetic spectra because the parameters of the atomic transitions come from theory or from laboratory experiments, and are not empirically calibrated with observed spectra.

Another possible source for these strong biases can be related to the different model atmospheres used. We have estimated the atmospheric parameters of the Sun with ZASPE+H13 finding that

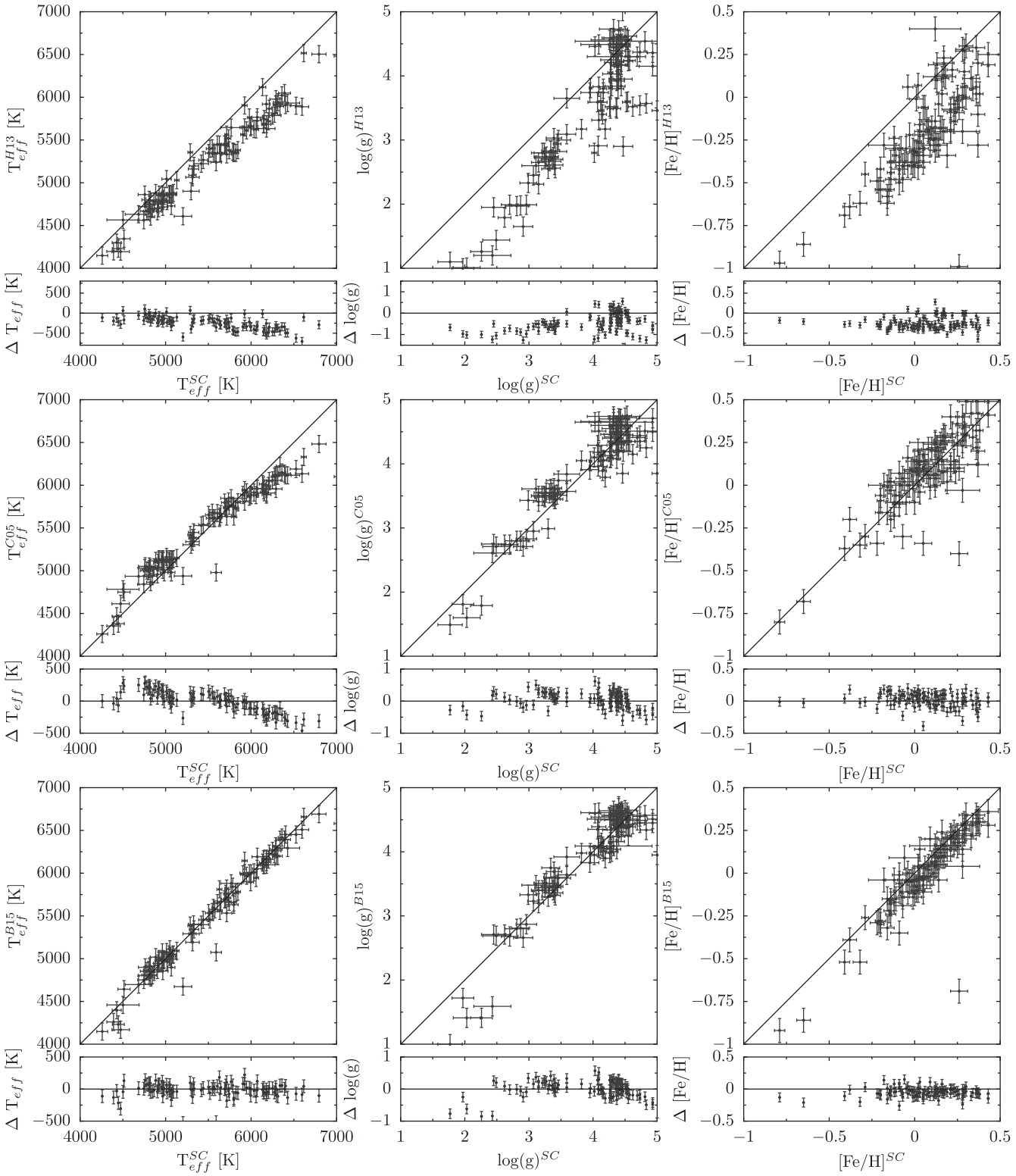

Figure 5. Comparison of the atmospheric parameters obtained by ZASPE using three different libraries of synthetic spectra against the values reported in SWEET-Cat. The top panels correspond to the results obtained using the H13 grid, where strong biases and systematic trends are present in the three parameters probably because the parameters of the atomic transitions were not empirically calibrated. The central panels correspond to the results obtained using the C05 grid, where a strong systematic trend in $T_{\rm eff}$ drives $T_{\rm eff}$ values towards that of the Sun. The bottom panels show the results obtained by ZASPE when using the synthetic library presented in this work. Results are compatible with the values reported in SWEET-Cat and no strong systematic trends can be identified.

they present important deviations with respect to the accepted reference values ($T_{\rm eff\odot}^{\rm H13} = 5430$ K, $\log g_{\odot}^{\rm H13} = 4.1$ dex, $[{\rm Fe/H}]_{\odot}^{\rm H13} = -0.3$ dex). These results show that if the strong observed biases are produced due to the use of different model atmospheres, the PHOENIX models are less precise than the ATLAS ones for estimating atmospheric parameters.

The central panels of Fig. 5 correspond to the results obtained by ZASPE using the C05 library. Even though the average values determined with the C05 grid are more compatible with the reference values than the ones obtained with the H13 grid, there is a strong trend in $\Delta T_{\rm eff}$. The systematic tends to bring the values of $T_{\rm eff}$ towards the one of the Sun (≈5750 K) and can produce deviations of ≈500 K for F-type stars. In this case both set of results are obtained using the same model atmospheres. The origin of the observed bias is unknown, but it can be plausibly related to two procedures that were adopted in the generation of the C05 grid. First, the oscillator strengths ($\log gf$) of several Fe transitions were calibrated using a high-resolution spectrum of the Sun, which could bias the results if the physical processes responsible for the formation of the lines are not accurately modelled by the synthesizing program; and second, all the spectra with $\log g > 3.0$ were synthesized assuming a solar microturbulence value of $v_{\rm t} = 1.0$ km s^{-1}, but FGK dwarfs have measured microturbulence values in the range of ≈0–6 km s^{-1}. The behaviour obtained for the values of the other parameters show less biases. However, the trend in $T_{\rm eff}$ coupled with the correlations in the atmospheric parameters induces an important dispersion in $\log g$ and [Fe/H]. The results obtained with these two grids of synthetic spectra show that in order to obtain reliable results, ZASPE requires an unbiased grid.

2.7 A new synthetic grid

As shown in the last section, it is not straightforward to use public libraries of synthetic spectra for estimating atmospheric parameters of stars due to strong systematic trends and biases that can arise due to erroneous physical assumptions and calibrations. For that reason, we decided to synthesize a new grid. We used the SPECTRUM code (Gray 1999) and the Kurucz model atmospheres (Castelli & Kurucz 2004) with solar scaled abundances. In order to avoid biases in $T_{\rm eff}$ related to assuming a fixed microturbulence value, we assume that the microturbulence is a function of $T_{\rm eff}$ and $\log g$. Ramírez, Allende Prieto & Lambert (2013) established an empirical calibration of the microturbulence as a function of the three atmospheric parameters but the validity of the proposed relation was limited to stars having $T_{\rm eff} > 5000$ K. We thus decided to base our microturbulence calibration on the values computed in SWEET-Cat by Santos et al. (2013). We considered only the systems having the homogeneity flag and by visually inspecting the dependence of the microturbulence with respect to the atmospheric parameters, we defined three different regimes for our empirical microturbulence law. For dwarf stars ($\log g > 3.5$), the microturbulence was assumed to depend on $T_{\rm eff}$ by a third-degree polynomial, while for subdwarf and giant stars, the microturbulence was fixed to two different values as follows:

$$v_{\rm t} = -36.125 + 0.019T_{\rm eff} - 3.65 \times 10^{-6}T_{\rm eff}^2 + 2.28 \times 10^{-10}T_{\rm eff}^3 \quad (\log g > 3.5),$$

$$v_{\rm t} = 1.2\,{\rm km\,s^{-1}} \quad (3.0 < \log {\rm g} < 3.5),$$

$$v_{\rm t} = 1.6\,{\rm km\,s^{-1}} \quad (\log {\rm g} < 3.0).$$

Table 2. Sample of stars with temperatures measured using interferometric observations (Boyajian et al. 2012, 2013) that were used to empirically calibrate $\log gf$ values and damping constants of prominent absorption lines.

Name	$T_{\rm eff}$ (K)	$\sigma_{T_{\rm eff}}$ (K)	$\log g$	[Fe/H]	Instrument
GJ 105	4662	17	4.52	−0.08	FEROS
GJ 166A	5143	14	4.54	−0.24	FEROS
GJ 631	5337	41	4.59	0.04	FEROS
GJ 702A	5407	52	4.53	0.03	FEROS
HD 102870	6132	26	4.11	0.11	FEROS
HD 107383	4705	24	2.61	−0.30	HIRES
HD 109358	5653	72	4.27	−0.30	HIRES
HD 115617	5538	13	4.42	0.01	FEROS
HD 131156	5483	32	4.51	−0.14	FEROS
HD 142860	6294	29	4.18	−0.19	FEROS
HD 145675	5518	102	4.52	0.44	HIRES
HD 1461	5386	60	4.20	0.16	FEROS
HD 146233	5433	69	4.25	−0.02	FEROS
HD 16895	6157	37	4.25	−0.12	HIRES
HD 182572	5787	92	4.23	0.33	FEROS
HD 19373	5915	29	4.21	0.09	HIRES
HD 20630	5776	81	4.53	0.0	FEROS
HD 210702	4780	18	3.11	0.03	HIRES
HD 222368	6288	37	3.98	−0.08	FEROS
HD 22484	5997	44	4.07	−0.09	FEROS
HD 30652	6516	19	4.30	−0.03	FEROS
HD 33564	6420	50	4.24	0.08	HIRES
HD 34411	5749	48	4.21	0.05	HIRES
HD 39587	5961	36	4.47	−0.16	FEROS
HD 4614	6003	24	4.39	−0.30	HIRES
HD 4628	4950	14	4.63	−0.22	FEROS
HD 7924	5075	83	4.56	−0.14	HIRES
HD 82328	6300	33	3.87	−0.12	HIRES
HD 82885	5434	45	4.39	0.06	HIRES
HD 86728	5612	52	4.26	0.20	HIRES
HD 90839	6233	68	4.41	−0.16	HIRES

We used the line list provided in the SPECTRUM code. We initially synthesized a grid of spectra using the original parameters of the transitions in the line list. However, after testing the grid with ZASPE we found that while the estimated $T_{\rm eff}$ and [Fe/H] values were closer to the Sweet-Cat ones than the values found using the other two public libraries, some slight but significant biases in these parameters were still present and also the $\log g$ values were strongly underestimated by ∼0.8 dex. For this reason, we decided to perform a similar approach to C05, and we tuned the $\log gf$ of several (∼400) prominent atomic lines. As opposed to C05, though, we did not use the spectrum of the Sun to perform the tuning, but instead we used the spectra of a set of stars that have some of their atmospherical parameters obtained using more direct procedures. In particular, we used stars whose $T_{\rm eff}$ were measured by long baseline interferometry (Boyajian et al. 2012, 2013) and another set of stars with $\log g$ values precisely determined through asteroseismology using *Kepler* data (Silva Aguirre et al. 2015). For the latter sample of stars, we obtained their spectra from the public Keck/High Resolution Echelle Spectrograph (HIRES) archive, while for the former sample, we obtained the spectra from the same archive but we also use data of the Fiber-fed Extended Range Optical Spectrograph (FEROS) spectrograph that was found in the ESO archive. Table 2 shows the stars that were used to adjust the $\log gf$ values. Even though the values for $T_{\rm eff}$ and $\log g$ are precisely determined for these stars, they can present important variations in their abundances. This factor is not

Table 3. Sample of stars with $\log g$ values measured using asteroseismology of *Kepler* data (Silva Aguirre et al. 2015) that were used to empirically calibrate $\log gf$ values and damping constants of prominent absorption lines.

Name	$T_{\rm eff}$ (K)	$\sigma_{T_{\rm eff}}$ (K)	$\log g$	$\sigma_{\log g}$	[Fe/H]	$\sigma_{\rm [Fe/H]}$	Instrument
KOI 1612	6104	74	4.293	0.004	−0.20	0.10	HIRES
KOI 108	5845	88	4.155	0.004	0.07	0.11	HIRES
KOI 122	5699	74	4.163	0.003	0.30	0.10	HIRES
KOI 41	5825	75	4.125	0.004	0.02	0.10	HIRES
KOI 274	6072	75	4.056	0.013	−0.09	0.10	HIRES
HIP 94931	5046	74	4.560	0.003	−0.37	0.09	HIRES
KOI 246	5793	74	4.280	0.003	0.12	0.07	HIRES
KOI 244	6270	79	4.275	0.008	−0.04	0.10	HIRES
KOI 72	5647	74	4.344	0.003	−0.15	0.10	HIRES
KOI 262	6225	75	4.135	0.008	−0.00	0.08	HIRES
KOI 277	5911	66	4.039	0.004	−0.20	0.06	HIRES
KOI 123	5952	75	4.213	0.008	−0.08	0.10	HIRES
KOI 260	6239	94	4.240	0.008	−0.14	0.10	HIRES
KOI 1925	5460	75	4.495	0.002	0.08	0.10	HIRES
KOI 5	5945	60	4.007	0.003	0.17	0.05	HIRES
KOI 245	5417	75	4.570	0.003	−0.32	0.07	HIRES
KOI 7	5781	76	4.102	0.005	0.09	0.10	HIRES
KOI 263	5784	98	4.061	0.004	−0.11	0.11	HIRES
KOI 975	6305	50	4.026	0.004	−0.03	0.10	HIRES
KOI 69	5669	75	4.468	0.003	−0.18	0.10	HIRES
KOI 42	6325	75	4.262	0.008	0.01	0.10	HIRES

directly included in the calibration procedure that is described in the following paragraphs, where just the [Fe/H] values are considered, which are furthermore less certain than the other two parameters. Nonetheless, as will be shown in the end of this section, the assumption that all these stars present small variations in their abundances is sufficient to significantly improve the performance of the calibrated grid of synthetic spectra.

For each absorption line, we determined the best $\log gf$ value in the case of each reference spectrum by building synthetic spectra in this particular spectral region with different values of $\log gf$ but with the stellar parameters fixed to the ones obtained by asteroseismology or interferometry. For each star, we found the synthetic spectrum that produces the smaller χ^2 and we save the $\log gf$ value of that model. Then we used the median value of the $\log gf$ determined for the different stars as the calibrated $\log gf$ value of the particular atomic transition.

In addition to the $\log gf$ values of the ∼400 spectral lines, we also manually adjusted the damping constants of the Mg Ib triplet and Na I doublet using a similar procedure. SPECTRUM uses the classical van der Waals formulation to generate the wings of the strong lines, but this procedure has been found to underestimate the strength of the absorption features. A common solution is to include an enhancement factor to correct for this behaviour. In our case, we determined this empirical adjustment factor for each of these strong lines using the above-mentioned set of standard stars. We found that the adjustment factor has a temperature dependence. Anstee & O'Mara (1991) developed a detailed approximation of the van der Waals theory in which the temperature dependence of the damping constant was determined to follow a power law. In our case, we empirically treated the temperature dependence of the damping constants by fitting linear relations to the enhancement factors determined from the standard stars as a function of the temperature for each strong line. These parameters were then used to synthesize the Mg Ib and Na I lines for spectra with different values of $T_{\rm eff}$. We assume at this point that the standard stars that we use for the calibration have similar Mg abundances. In addition, the synthetic spectra that are generated following this calibration procedure may show some systematic biases when using them to determine the $\log g$ values stars having non-solar Mg abundances (see Brewer et al. 2015).

The spectral range of our grid goes from 4900 to 6100 Å. This range was selected because most of the spectral transitions for FGK-type stars are located at shorter wavelengths than 6000 Å but for $\lambda < 5000$ Å spectral lines become excessively crowded that complicates the process of adjusting the $\log gf$ values. The grid limits and spacings of the stellar parameters of the grid we synthesized are

(i) $T_{\rm eff}$: 4000–7000 K, $\Delta T_{\rm eff} = 200$ K;
(ii) $\log g$: 1.0–5.0 dex, $\Delta \log g = 0.5$ dex;
(iii) [Fe/H]: −1.0–0.5 dex, Δ[Fe/H] = 0.25 dex.

We used a multidimensional cubic spline to generate the model atmospheres with atmospheric parameters not available in the original set of atmospheres provided by the Kurucz models.

The bottom panels of Fig. 5 show the results obtained using ZASPE with this new grid of synthetic spectra against the values stated in SWEET-Cat. The results agree very well with the reference values and no evident trends are present. The $T_{\rm eff}$ shows an excellent agreement with only two outliers at present. The results obtained for $\log g$ have some tentative systematic trends. In particular, we note that SWEET-Cat report some $\log g$ values greater than 4.7 dex, but we note that surface gravities higher than that are not common for FGK-type stars so those values are suspect. The [Fe/H] values present no offset trends, but a systematic bias can be identified. [Fe/H] values are on average underestimated by 0.05 dex as compared to the SWEET-Cat values. However, differences of ≈0.09 dex in [Fe/H] have been previously reported when comparing SWEET-Cat metallicities against the ones computed with the ones obtained via spectral synthesis techniques, so the offset we observe is within the expected range given the different techniques used (Mortier et al. 2013). In order to further check the performance of our new grid we used other three different samples of stars with stellar parameters obtained in a homogeneous way. First, we used our two sets of stars with stellar parameters obtained using

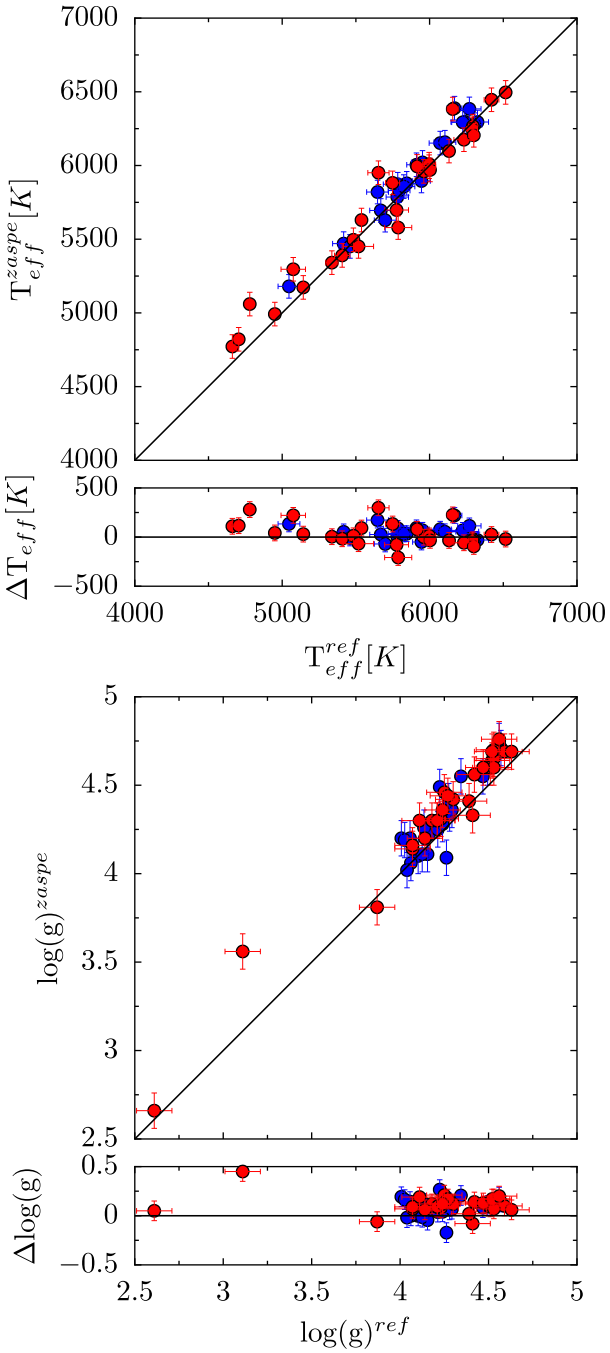

Figure 6. Comparison between the parameters obtained by ZASPE using the new grid and the reference values for the sets of stars with asteroseismological (blue) and interferometric (red) derived parameters. The upper panel shows the results in the case of $T_{\rm eff}$ and the lower panel for $\log g$.

interferometry and asteroseismology that are shown in Tables 2 and 3. Fig. 6 shows the comparison of the parameters obtained using ZASPE with our new grid as function of the reference values. We only plot $T_{\rm eff}$ and $\log g$ because only these two parameters are measured directly using interferometry and asteroseismology, respectively. The third sample of stars that we use corresponds to the exoplanet host stars analysed by Torres et al. (2012), where the $\log g$ values where precisely obtained by using the measured stellar densities obtained from the transit light curve. Fig. 7 shows the results obtained by ZASPE as function of the parameters found in the mentioned study. For these three samples of stars, the parameters obtained with ZASPE using our new grid are in good agreement with the reference values. However, there is still a slight but significant overestimation of the $\log g$ values in the case of dwarf stars. This problem can be produced because (i) not all the spectral lines were empirically calibrated, and (ii) we are imposing that the modelling errors are originated from unreliable $\log gf$ values, and therefore, when we perform the calibration that significantly improves the quality of the synthetic grid, some additional weaker systematic errors could be introduced.

Our new spectral library has been made publicly available.[3]

3 PERFORMANCE

As an example of the performance of ZASPE, we present here the results we obtain when using it to analyse the spectra of the Sun and Arcturus. The spectra of these two objects have been studied extensively and they are used commonly to calibrate and validate spectral studies of stars. We obtained raw data from the ESO archive for both stars observed with the FEROS spectrograph (Kaufer & Pasquini 1998). We processed them through an automated reduction and extraction pipeline we have developed for FEROS and other echelle spectrographs (Jordán et al. 2014; Brahm, Jordán & Espinoza 2016b). The grid of synthetic spectra used by ZASPE in this analysis was generated by us and is described in Section 2.7. The spectral range selected for analysing the data was from 5000 to 6000 Å, which ensures a great amount of spectral transitions including the Mg I triplet, which is the most pressure sensitive feature for dwarf stars. Figs 8 and 9 summarize the results we obtain. The left-hand panels show Hess diagrams in various planes using the outcome of the random sampling realizations, while the right-hand panels show the marginalized distribution functions of the stellar atmospheric parameters. The best-fitting parameters are marked with red circles in the panels on the left and vertical red lines in the ones on the right. Reference values of the stellar parameters are marked with blue circles in the panels on the left and blue lines in the ones on the right.

In the case of the Sun, the best-fitting parameters and errors we obtained were $T_{\rm eff} = 5818 \pm 59$ K, $\log g = 4.49 \pm 0.09$ dex and $[{\rm Fe/H}] = 0.01 \pm 0.04$ dex. These results are compatible with the accepted parameters of the Sun being 0.8σ, 0.6σ and 0.3σ apart in $T_{\rm eff}$, $\log g$ and [Fe/H], respectively. The results obtained for Arcturus were $T_{\rm eff} = 4331 \pm 63$ K, $\log g = 1.68 \pm 0.25$ dex and $[{\rm Fe/H}] = -0.48 \pm 0.09$ dex. In Fig. 9, we include the parameters computed by Meléndez et al. (2003) that are compatible with the results obtained by ZASPE at the 1σ level.

In both cases, ZASPE shows there is a wide spread of possible outcomes that confirms the idea that the principal source of uncertainty is the imperfect modelling of the synthesized spectra. The uncertainties in the parameters that ZASPE reports are computed from the standard deviation of the values obtained in the random sampling simulations. The uncertainties in the parameters we found for the Sun are smaller than the ones found for Arcturus. This serves to illustrate that the amplitude of the uncertainty in the atmospheric parameters varies with spectral type, and that the synthetic grid we used has a better calibration for dwarf stars than for giant stars. It is therefore not accurate to adopt universal minimum uncertainties, as is often done in the literature.

[3] http://www.astro.puc.cl/~rbrahm/new_grid.tar.gz

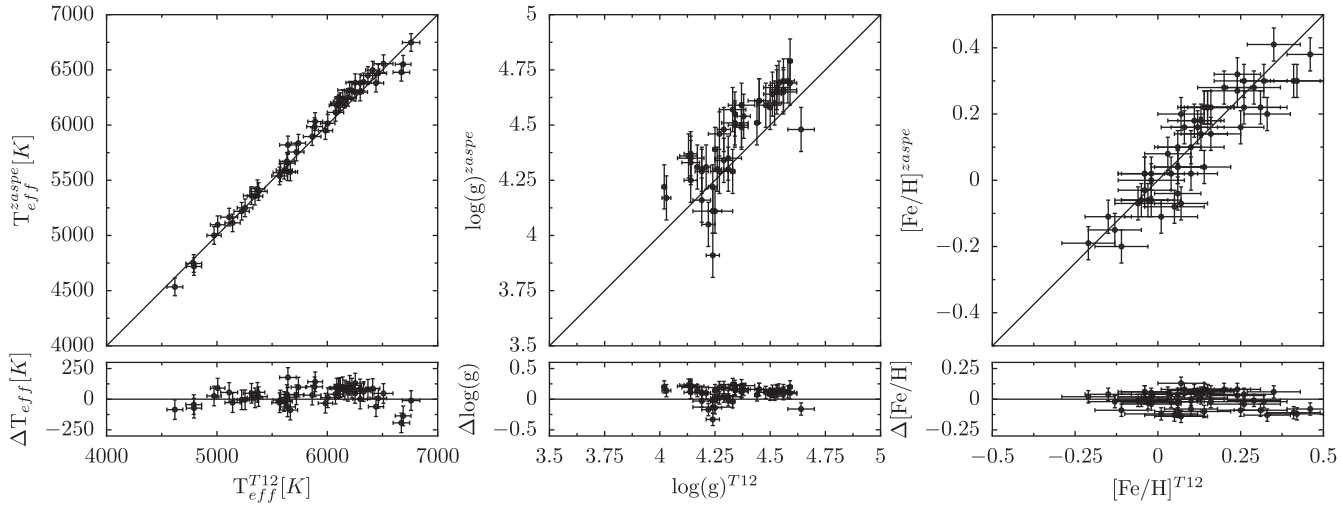

Figure 7. Comparison between the parameters obtained by ZASPE using the new grid and the reference values for the set of stars analysed in Torres et al. (2012). Left, central and right-hand panels correspond to the comparisons in $T_{\rm eff}$, $\log g$ and [Fe/H], respectively.

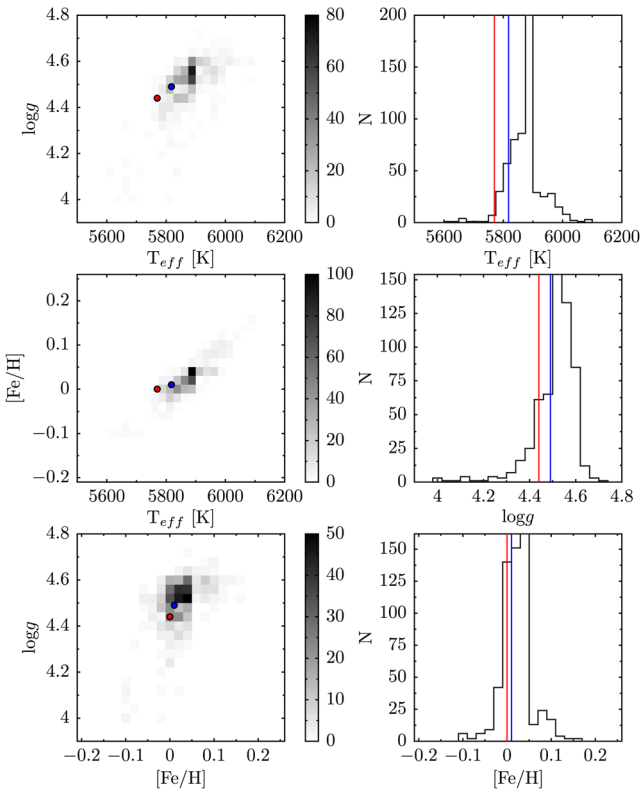

Figure 8. Results obtained by ZASPE for the Sun. The left-hand panels show the distribution of possible sets of atmospheric parameters obtained from the random sampling method. Strong correlations between the parameters are found. The blue circles correspond to the parameters of the synthetic spectrum that produce the best match, while the red circles are reference values from the literature. The right-hand panels correspond to the marginalized distributions of outcomes for each atmospheric parameter. Blue lines show the parameters of the synthetic spectrum that produce the best match, while red lines are the reference values. The errors reported by ZASPE correspond to the standard deviations of these distributions.

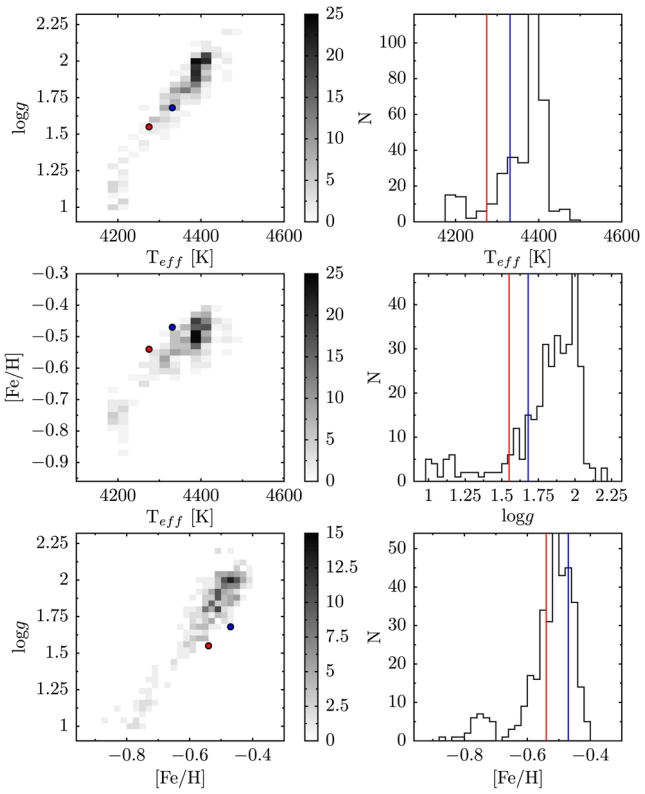

Figure 9. Same as Fig. 8 but for Arcturus.

The left-hand panels of Figs 8 and 9 also show the existence of strong correlations between the parameters. The Pearson correlation coefficients ρ between the parameters in the case of the Sun are $\rho_{T_{\rm eff}-\log g} = 0.63$, $\rho_{T_{\rm eff}-[{\rm Fe/H}]} = 0.89$ and $\rho_{\log g-[{\rm Fe/H}]} = 0.49$. For Arcturus, the correlations we found are $\rho_{T_{\rm eff}-\log g} = 0.95$, $\rho_{T_{\rm eff}-[{\rm Fe/H}]} = 0.87$ and $\rho_{\log g-[{\rm Fe/H}]} = 0.92$.

One first thing to note about the performance of ZASPE on the Sun and Arcturus, beyond the fact that the resulting stellar parameters are consistent with known values produced by current state-of-the-art

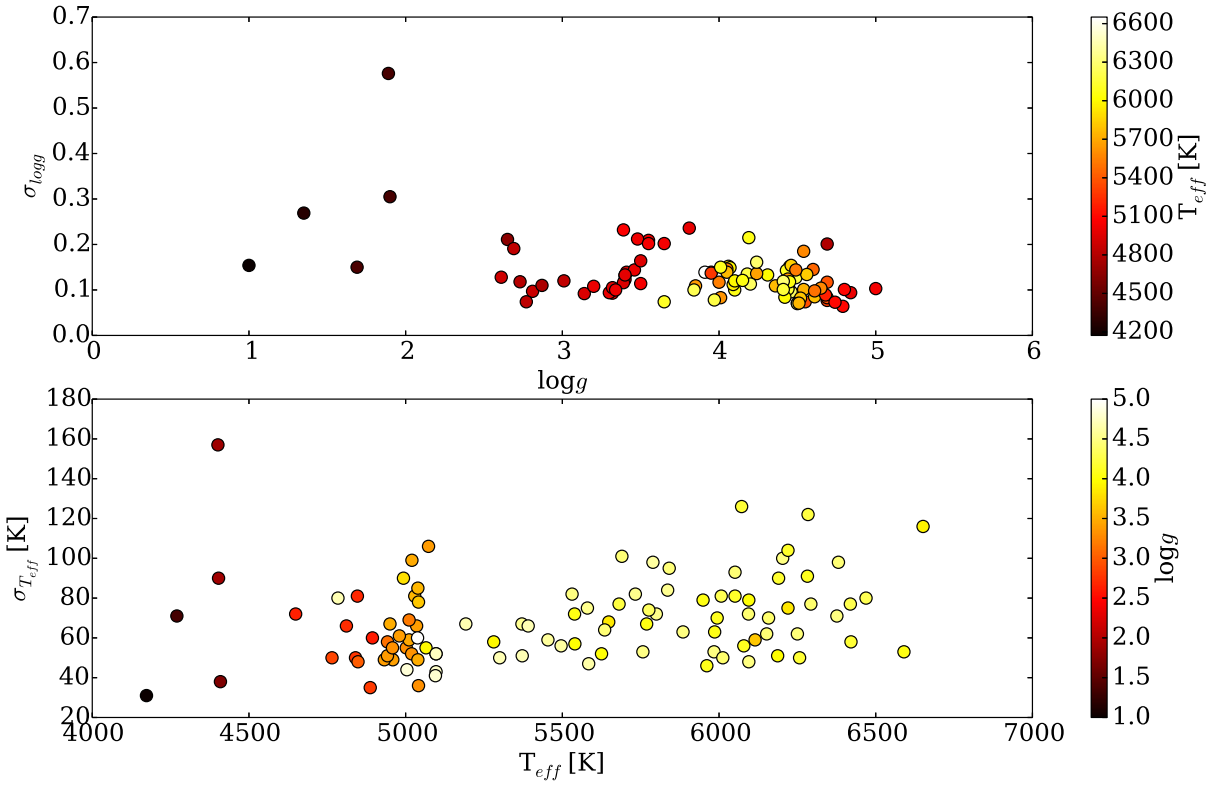

Figure 10. Top: errors in log g reported by ZASPE as function of the log g values. Dwarfs stars have in general smaller errors than giant stars. Bottom: errors in $T_{\rm eff}$ reported by ZASPE as function of the $T_{\rm eff}$ values. In the case of dwarf stars, hotter stars tend to have larger errors.

analyses, is the magnitude of the uncertainties. Despite the very high SNR of the spectra, the estimated uncertainties in $T_{\rm eff}$ are ∼50 K. This compares very well with the uncertainty of $\sigma_{T_{\rm eff}} = 59$ K that Torres et al. (2012) add in quadrature to their formal uncertainties. This uncertainty is obtained from the overall scatter of their measurements for stars with multiple determinations obtained with different methods (SPC, SME and/or MOOG). In the same vein, the uncertainties in [Fe/H] for the Sun[4] are of order ∼0.05 dex, compared with the value of $\sigma_{\rm [Fe/H]} = 0.062$ adopted by Torres et al. (2012). From this exercise, we can see that the uncertainties returned by ZASPE are a realistic reflection of the model uncertainties that dominate in our case. As opposed to the methods based on repeated measurements on a sample of objects, ZASPE can provide the uncertainty on as per spectrum basis, and also provides the correlation with other parameters.

In order to explore how the magnitude of the computed errors depend on the atmospheric parameters, we analysed the results that were obtained by ZASPE on the data set presented in Section 2.7, where we obtained the atmospheric parameters and their associated errors for a set of FEROS spectra of stars that have been already analysed by SWEET-Cat. From this sample, we conclude that there is no strong dependence between the magnitude of the errors that we estimate and the atmospheric parameters of the star. However, there are two tentative trends that are shown in Fig. 10. The top panel of the figure shows that dwarf stars tend to have lower errors in log g than giant stars. The origin of this correlation can be associated with the tight pressure sensitivity of the shape of the wings of strong absorption lines, which is only present in dwarf stars. In the case of giant stars, the principal factor that produces variation in log g are subtle changes in the depth of shallow lines generated from variations in the continuum absorption. The bottom panel of Fig. 10 shows that for dwarf stars, the $T_{\rm eff}$ errors computed by ZASPE tend to be higher or at least have a larger dispersion for hotter stars, which can arise from the higher rotational velocity F-type stars have in comparison to G-type stars, but also because at higher temperatures ($T_{\rm eff} > 6000$ K), a large fraction of the elements in the atmosphere start to get ionized and therefore there are less available absorption lines. Another possible reason for having a larger dispersion in $T_{\rm eff}$ for hotter stars is that at these temperatures the strong lines become less sensitive to changes in pressure. This can produce a higher uncertainty in $T_{\rm eff}$ due to the strong correlations between the parameters. However, the reported trends of both panels show important levels of scatter. In particular, there is a cluster of stars with $T_{\rm eff} \approx 5000$ K, log $g \approx 3.5$ dex and similar [Fe/H] values that shows a large scatter in the magnitude of their errors. The source of this dispersion may be associated with other systematic effects, like differences in particular abundances or incorrect assumptions in the micro- and macroturbulence values.

As a further example of the performance of ZASPE, we analysed an archival Keck/HIRES (Vogt et al. 1994) spectrum of WASP-14. We chose this star as it is representative of the use of atmospheric parameter estimation in the process of discovery and characterization of exoplanets, which was the main motivation for developing ZASPE. Additionally, WASP-14 was analysed with STARFISH by Czekala et al. (2015). As STARFISH is the only other approach we are aware of that attempts to properly take into account the model uncertainties as we do in this work, it offers a very interesting point of comparison. Czekala et al. (2015) estimate the stellar parameters of WASP-14

[4] The [Fe/H] uncertainty for Arcturus is higher by a factor of ≈2. This is a consequence of the less constrained value of log g for a giant, which has an impact on the uncertainty of [Fe/H].

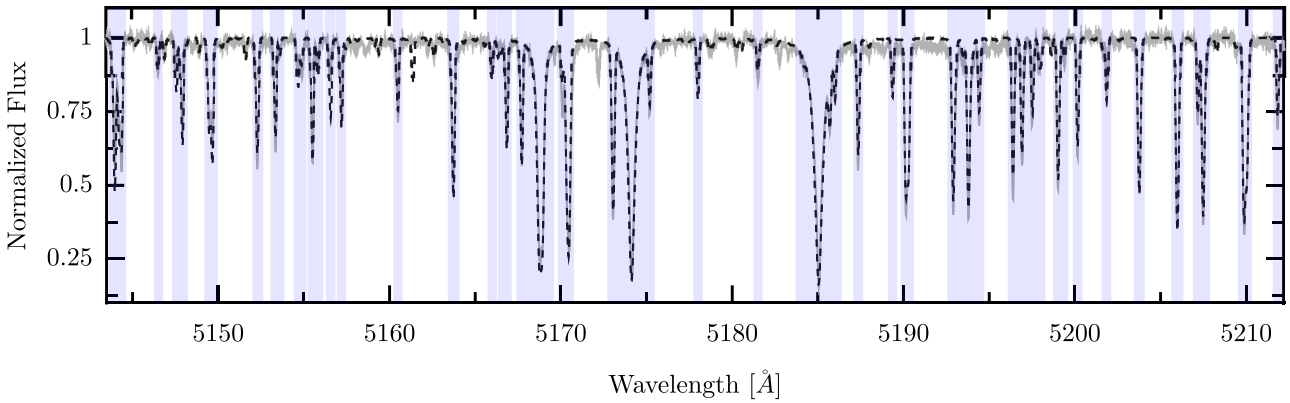

Figure 11. A portion of the spectrum of WASP-14 observed with Keck/HIRES in the zone of the Mg Ib triplet. The grey line corresponds to the observed spectrum, while the dashed line is the synthetic spectrum with atmospheric parameters determined by ZASPE. Shaded in blue are the sensitive zones that ZASPE selected.

using a spectrum from the Tillinghast Reflector Echelle Spectrograph (TRES) spectrograph on the Fred Lawrence Whipple Observatory 1.5-m telescope and fixing $\log g$ to the value obtained by Torres et al. (2012) by fitting the transit light curve, namely $\log g = 4.29$. They estimate parameters using both Kurucz and PHOENIX stellar atmospheric models. The STARFISH estimates and their uncertainties are presented in their table 1 and are (values using Kurucz models) $T_{\rm eff} = 6426 \pm 21$ K, [Fe/H] $= -0.26 \pm 0.01$ and $v \sin i = 4.47 \pm 0.06$ km s^{-1}.

Running ZASPE on the Keck/HIRES spectrum with fixed $\log g = 4.29$ results in the following estimates: $T_{\rm eff} = 6515 \pm 64$ K, [Fe/H] $= -0.15 \pm 0.04$ and $v \sin i = 5.55 \pm 0.37$ km s^{-1}. Again, the uncertainties are reasonable based on what is expected from studies that have obtained measurements with different methods such as Torres et al. (2012), and are actually made somewhat artificially low by fully fixing $\log g$.[5] The difference with the uncertainties obtained by STARFISH is substantial, with the STARFISH uncertainties being underestimated based on the experience provided by studies such as that of Torres et al. (2012). This is also clear from comparing the parameters derived by STARFISH on the same data using different stellar models, as they are in some cases formally inconsistent given their error bars, something that should not be the case if the uncertainties arising from model imperfections have been properly estimated. Fig. 11 shows a portion of the HIRES spectrum of WASP-14 and the synthetic spectrum with the optimal parameters derived by ZASPE. The sensitive zones determined by ZASPE are shaded blue.

It is worthwhile trying to understand why the approach of Czekala et al. (2015) leads to underestimated uncertainties. Their approach is very principled, and being immersed in a likelihood, it is very appealing for inference. Their approach takes into account the mismatches between models and data through modelling the variance structure with a Gaussian process. To that effect, a mixture of non-stationary kernels that indicate regions of very strong deviation, and a stationary global kernel, is used. The non-stationary kernels, with large variances, have the effect of ignoring regions where those kernels are instantiated, and is a way of eliminating lines that are outliers in a principled way. The stationary kernel accounts for the typical mismatch between the model and the data, and it is chosen to be of the form of a Matérn $\nu = 3/2$ kernel, tapered by a Hann window function to keep the global covariance matrix sparse. In this approach, the possible mismatches between the model and the data are given by the space of functions generated by the Matérn $\nu = 3/2$ kernel with the hyperparameter distributions learned in the inference process.

The key observation is that the mismatches are not appropriately described by a stationary kernel, as they ought to exist mostly around the lines, and thus the process that would be needed to account for the mismatch structure is fundamentally non-stationary. In our re-sampling scheme, we just modify the depth of the lines, exploring thus systematically variations in the models that have physical plausibility. Variations given by a stationary Gaussian kernel will have no correlation with the line structure, and would be therefore mostly unphysical. This can be seen in the right-hand panels of fig. 4 in Czekala et al. (2015), the random draws from the stationary kernel have structure on locations that are uncorrelated with the spectral lines. The stationary kernel encapsulates the typical covariance structure of the mismatch, including large swaths of the spectrum that are continuum where little mismatch is observed, as those regions are less sensitive to the parameters. One expects then that the amplitude of the variance is a sort of average description of continuum and line regions, and would thus underestimate the variance at the more relevant regions of the spectral lines. In summary, we believe the inability of STARFISH to deliver realistic uncertainties is due to fact that their use of a Matérn $\nu = 3/2$ kernel is not necessarily expected to correctly describe the functional space of mismatches and the variance amplitude relevant at the location of spectral lines.

4 SUMMARY

In this work, we have presented a new algorithm based on the spectral synthesis technique for estimating stellar atmospheric parameters of FGK-type stars from high-resolution echelle spectra. The comparison between the data and the models is performed iteratively in the most sensitive zones of the spectra to changes in the atmospheric parameters. These zones are determined after each ZASPE iteration and the regions of the spectra that strongly deviate from the best model are not considered in future iterations.

ZASPE computes the errors and correlations in the parameters from the data itself by assuming that the uncertainties are dominated by the systematic mismatches between the data and the models that arise from unknown parameters of the particular atomic transitions.

[5] The stellar parameters obtained leaving $\log g$ free are $T_{\rm eff} = 6501 \pm 134$ K, [Fe/H] $= -0.17 \pm 0.07$, $v \sin i = 5.58 \pm 0.5$ km s^{-1} and $\log g = 4.22 \pm 0.18$.

These systematic effects manifest themselves by randomly modifying the strength of the absorption lines of the synthesized spectra. The distribution of mismatches is determined by ZASPE from the observed spectra and the synthetic model that produces the best fit. A random sampling method uses an empirical distribution of line strength mismatches to modify the complete grid of synthetic spectra in a number of realizations and a new set of stellar parameters is determined in each realization. The complete covariance matrix can be computed from the distribution of outputs of the random sampling method.

We have validated ZASPE by comparing its estimates with the SWEET-Cat catalogue of stellar parameters. We have found that the synthetic libraries of C05 and H13 are not suitable for obtaining reliable atmospheric parameters because they present some strong systematic trends when comparing ZASPE results obtained with these grids against SWEET-Cat reference values. We have detailed the methodology to generate our own library of synthetic spectra that we have shown is able to obtain consistent results with the SWEET-Cat catalogue. We have estimated stellar parameters for the Sun and Arcturus using high SNR archival spectra, obtaining results consistent with state-of-the-art estimates for these archetypical stars. Importantly, we obtain uncertainties that are in line with the expected level of systematic uncertainties based on studies that have performed repeat measurements of a sample of stars. Finally, we have estimated parameters for the star WASP-14, as both a way to gauge performance on a typical star that is followed-up in exoplanetary transit surveys and to compare to the STARFISH code, the only other approach that we are aware of that deals with the systematic mismatch between models and data. Unlike ZASPE the STARFISH code delivers underestimated uncertainties, a fact we believe is due to the modelling of the mismatch structure using a stationary kernel for what is fundamentally a non-stationary process as it is concentrated in the line structure.

Currently ZASPE works for stars of spectral type FGK. The main barriers to extend the use of ZASPE for stars with lower $T_{\rm eff}$ are related to the assumption that the systematic mismatches can be modelled by one random variable that modifies the strength of the absorption lines. Molecular bands become the principal feature in the spectra for stars with $T_{\rm eff} < 4000$ K, and a more complex model is required to characterize the systematic differences between observed and synthetic spectra. Extension to later types will be the subject of future efforts.

ZASPE is mostly a PYTHON-based code with some routines written in C. It has the option of being run in parallel with the user having the capability of entering the number of cores to be utilized. On a 16 core CPU, it takes ≈10 min for ZASPE to find the synthetic spectrum that produces the best match with the data. However, to determine the covariance matrix, a couple of hours are required. ZASPE has been adopted as the standard procedure for estimating the stellar atmospheric parameters of the transiting extrasolar systems discovered by the HATSouth survey (Bakos et al. 2013); to date its results have been used for the analysis of 27 new systems (from HATS-9b to HATS-35b; Brahm et al. 2015, 2016a; Mancini et al. 2015; Bento et al. 2016; Bhatti et al. 2016; Ciceri et al. 2016; de Val-Borro et al. 2016; Espinoza et al. 2016; Penev et al. 2016; Rabus et al. 2016). ZASPE is made publicly available at http://github.com/rabrahm/zaspe.

ACKNOWLEDGEMENTS

RB is supported by CONICYT-PCHA/Doctorado Nacional. RB acknowledges additional support from project IC120009 'Millennium Institute of Astrophysics (MAS)' of the Millennium Science Initiative, Chilean Ministry of Economy. AJ acknowledges support from FONDECYT project 1130857, BASAL CATA PFB-06 and project IC120009 'Millennium Institute of Astrophysics (MAS)' of the Millennium Science Initiative, Chilean Ministry of Economy.

REFERENCES

Anstee S. D., O'Mara B. J., 1991, MNRAS, 253, 549
Bakos G. Á. et al., 2013, PASP, 125, 154
Bento J. et al., 2016, MNRAS, in press, preprint (arXiv:1607.00688)
Bhatti W. et al., 2016, AAS Meeting, preprint (arXiv:1607.00322)
Blanco-Cuaresma S., Soubiran C., Heiter U., Jofré P., 2014, A&A, 569, A111
Boyajian T. S. et al., 2012, ApJ, 757, 112
Boyajian T. S. et al., 2013, ApJ, 771, 40
Brahm R. et al., 2015, AJ, 150, 33
Brahm R. et al., 2016a, AJ, 151, 89
Brahm R., Jordán A., Espinoza N., 2016b, PASP, in press preprint (arXiv:1609.02279)
Brewer J. M., Fischer D. A., Basu S., Valenti J. A., Piskunov N., 2015, ApJ, 805, 126
Buchhave L. A. et al., 2012, Nature, 486, 375
Buchhave L. A. et al., 2014, Nature, 509, 593
Burke C. J. et al., 2014, ApJS, 210, 19
Castelli F., Kurucz R. L., 2004, preprint (astro-ph/0405087)
Ciceri S. et al., 2016, PASP, 128, 074401
Coelho P., Barbuy B., Meléndez J., Schiavon R. P., Castilho B. V., 2005, A&A, 443, 735 (C05)
Czekala I., Andrews S. M., Mandel K. S., Hogg D. W., Green G. M., 2015, ApJ, 812, 128
de Val-Borro M. et al., 2016, AJ, 152, 161
Espinoza N., Jordán A., 2015, MNRAS, 450, 1879
Espinoza N. et al., 2016, AJ, 152, 108
Gray R. O., 1999, Astrophysics Source Code Library, record ascl:9910.002
Gray D. F., 2008, The Observation and Analysis of Stellar Photospheres. Cambridge Univ. Press, Cambridge
Grunhut J. H., 2009, Master's thesis, Queen's University. Available at: http://hdl.handle.net/1974/1707
Howard A. W. et al., 2010, Science, 330, 653
Howard A. W. et al., 2012, ApJS, 201, 15
Husser T.-O., Wende-von Berg S., Dreizler S., Homeier D., Reiners A., Barman T., Hauschildt P. H., 2013, A&A, 553, A6 (H13)
Jordán A. et al., 2014, AJ, 148, 29
Kaufer A., Pasquini L., 1998, in D'Odorico S., ed., Proc. SPIE Conf. Ser. Vol. 3355, Optical Astronomical Instrumentation. SPIE, Bellingham, p. 844
Kurucz R. L., 1993, VizieR Online Data Catalog, 6039, 0
Mancini L. et al., 2015, A&A, 580, A63
Meléndez J., Barbuy B., Bica E., Zoccali M., Ortolani S., Renzini A., Hill V., 2003, A&A, 411, 417
Mortier A., Santos N. C., Sousa S. G., Fernandes J. M., Adibekyan V. Z., Delgado Mena E., Montalto M., Israelian G., 2013, A&A, 558, A106
Penev K. et al., 2016, AJ, 152, 127
Rabus M. et al., 2016, AJ, 152, 88
Ramírez I., Allende Prieto C., Lambert D. L., 2013, ApJ, 764, 78
Santos N. C. et al., 2013, A&A, 556, A150
Silva Aguirre V. et al., 2015, MNRAS, 452, 2127
Takeda Y., Sato B., Murata D., 2008, PASJ, 60, 781
Torres G., Fischer D. A., Sozzetti A., Buchhave L. A., Winn J. N., Holman M. J., Carter J. A., 2012, ApJ, 757, 161
Valenti J. A., Fischer D. A., 2005, ApJS, 159, 141
Valenti J. A., Piskunov N., 1996, A&AS, 118, 595
Vogt S. S. et al., 1994, in Crawford D. L., Craine E. R., eds, Proc. SPIE Vol. 2198, Instrumentation in Astronomy VIII. SPIE, Bellingham, p. 362

This paper has been typeset from a TEX/LATEX file prepared by the author.